



Palladium-nanoparticles on end-functionalized poly(lactic acid)-based stereocomplexes for the chemoselective cinnamaldehyde hydrogenation: Effect of the end-group



Werner Oberhauser^{a,*}, Claudio Evangelisti^{b,*}, Ravindra P. Jumde^b, Giorgio Petrucci^c, Mattia Bartoli^c, Marco Frediani^c, Matteo Mannini^d, Laura Capozzoli^e, Elisa Passaglia^f, Luca Rosi^c

^a Istituto di Chimica dei Composti Organometallici (CNR-ICCOM), Via Madonna del Piano 10, 50019 Sesto Fiorentino, Italy

^b Istituto di Scienze e Tecnologie Molecolari (CNR-ISTM), Via Fantoli 16/15, 20138 Milano, Italy

^c Dipartimento di Chimica, Università Degli Studi di Firenze, via della Lastruccia 13, 50019 Sesto Fiorentino, Italy

^d Laboratory of Molecular Magnetism, Dipartimento di Chimica Ugo Schiff, Università Degli Studi di Firenze and INSTM RU of Firenze, Via della Lastruccia 3, 50019 Sesto Fiorentino, Italy

^e Centro di Microscopia Elettronica (Ce.M.E.), Area di Ricerca CNR di Firenze, Via Madonna del Piano 10, 50019 Sesto Fiorentino, Italy

^f CNR-ICCOM, UOS Pisa, Area della Ricerca, Via Moruzzi 1, 56124 Pisa, Italy

ARTICLE INFO

Article history:

Received 13 March 2015

Revised 1 July 2015

Accepted 4 July 2015

Keywords:

Poly(lactic acid)

Stereocomplex

Pd-nanoparticles

Hydrogenation

Cinnamaldehyde

ABSTRACT

Differently carboxylic acid end-functionalized poly(lactic acid) (PLA)-based stereocomplexes were used as polymer support to stabilize Pd-nanoparticles (NPs) generated by the metal vapor synthesis technique. The dispersion of Pd was strongly dependent on the end-group present in the polymer structure, as shown by HRTEM measurements. 2,2'-Bipyridine- and pyridine-based stereocomplexes showed high metal dispersion (*i.e.* well-separated Pd-NP size of 2.0 ± 0.6 nm), whereas stereocomplexes bearing benzyl and carboxylic acid end groups exhibited strong Pd-NPs aggregation. The heterogeneous catalysts were employed to chemoselectively hydrogenate the C=C double bond in cinnamaldehyde, showing for Pd-NPs, stabilized by the 2,2'-bipyridine-modified polymer support, the best performance in terms of chemoselectivity (99%) and recyclability in THF solution. Even under bulk cinnamaldehyde hydrogenation conditions, chemoselectivity for 3-phenylpropanal of 90% at 88% conversion was obtained.

© 2015 Elsevier Inc. All rights reserved.

1. Introduction

The selective hydrogenation of the C=C double bond in α,β -unsaturated carbonyl compounds is an important organic transformation leading to the saturated counterparts which are widely applied in synthetic and pharmaceutical chemistry [1–3]. Metallic palladium embedded in a carbon support is generally used to catalyze the latter substrate conversion, which is not always chemoselective [4–7]. The support, which functions as macroligand, notably influences the electron density of the surface atoms of the Pd nanoparticles (NPs), thus allowing to promote a specific chemoselectivity. The graphitic structure of carbon, for instance, increases the charge density on the NP-surface [8]. As a consequence, the binding energy of the C=C bond in α,β -unsaturated carbonyl compounds decreases due to repulsive four-electron interactions, whereas the C=O bond hydrogenation is fostered by

the favored back-bonding interaction of the Pd-NPs with the π^*CO -orbital [8].

Alternatively to carbon supports, organic polymers [9,10], such as polyamines [11] and polyketones [12], endowed with functional groups that interact with the metal-NPs' surface, have shown to be a promising alternative support material for metal Pd-NPs, used in the hydrogenation of the structure-sensitive cinnamaldehyde to 3-phenylpropanal. Chemoselectivity in the range between 84% and 88% has been observed with the latter catalysts [11,12].

Recently we introduced the stereocomplex of 2,2'-bipyridine-functionalized poly(lactic acid) PLA as organic support for Pd-NPs, which selectively catalyzed the partial hydrogenation of phenylacetylene and diphenylacetylene [13]. The stereocomplex, which is formed upon hydrogen bond interactions between *l*- and *d*-PLA [14], is much more resistant against hydrolytic [15,16] and thermal degradation [17] compared to *l*- or *d*-PLA.

Herein we report the synthesis of differently end-functionalized PLA-based stereocomplexes, which were subsequently employed to stabilize Pd-NPs generated by metal vapor synthesis (MVS) technique [18,19]. The obtained heterogeneous polymer-based

* Corresponding authors.

E-mail addresses: werner.oberhauser@iccom.cnr.it (W. Oberhauser), claudio.evangelisti@istm.cnr.it (C. Evangelisti).

catalysts were used in the chemoselective C=C double bond hydrogenation of cinnamaldehyde to 3-phenylpropanal. Pd-NP dispersion and chemoselectivity of the catalytic reactions were notably influenced by the nature of the end-group present in the polymer back bond.

2. Experimental

2.1. Materials and apparatus

Tin octanoate ($\text{Sn}(\text{Oct})_2$) 4-hydroxymethylpyridine, benzylalcohol, 4-methyl-4'-(hydroxymethyl)-2,2'-bipyridine and *l*-lactide and *d*-lactide were purchased from Aldrich. *l*-lactide and *d*-lactide were sublimated before utilization and stored thereafter at 4 °C under nitrogen atmosphere. Solvents such as *n*-hexane, CHCl_3 , CDCl_3 and HPLC-grade THF were purchased from Aldrich and used without further purification. Mesitylene and *n*-hexane were purified by conventional methods, distilled and stored under nitrogen. The co-condensation of palladium and the appropriate solvent was carried out in a previously described static reactor [18,20].

^1H NMR spectra were recorded on a Bruker Avance DPX 300 spectrometer, measuring at 300.13 MHz, while $^{13}\text{C}\{^1\text{H}\}$ NMR spectra were obtained with a Bruker Avance DRX-400 spectrometer, acquiring at 100.62 MHz.

ATR-IR spectra were recorded on a Shimadzu model IR-Affinity apparatus, equipped with a Golden Gate single reflection diamond ATR accessory.

Gel-Permeation Chromatography (GPC) was carried out with a Waters Binary HPLC 1525 pump, a manual injector with a six way valve and a 200 μL loop, three Shodex KF-802, KF-803 and KF-804 columns connected in series (length: 300 mm each, inner diameter: 8.0 mm, 24,500 theoretical plates, exclusion limit for polystyrene (PS) up to 400,000 g mol^{-1} ; a refraction index (RI) detector (Optilab T-rEXTM, Wyatt Technology) and a UV detector (Waters mod. 2489)). HPLC-grade THF with a water content of maximal 0.1 vol% was used as eluent at a constant flow of 1.0 mL min^{-1} , keeping the columns at 30.0 °C with a thermostat. The GPC system was calibrated using PS as standard. Samples were prepared by dissolving 5.0 mg of analyte in 1.0 mL of eluent. The obtained solution was filtered through a 0.2 μm PTFE filter and injected.

GC analyses were performed with a Shimadzu 2010 gas chromatograph equipped with a flame ionization detector and a 30 m (0.25 mm i.d., 0.25 μm film thickness) VF-WAXms capillary column.

GC-MS analyses were performed with a Shimadzu QP5000 apparatus, equipped with a 30 m (0.32 mm i.d., 0.50 μm film thickness) CP-WAX 52CB WCOT-fused silica column.

High resolution transmission electron microscopy (HRTEM) analyses of the supported Pd-NPs were carried out with a ZEISS LIBRA 200FE HRTEM instrument, equipped with a FEG source operating at 200 kV, in column second-generation omega filter for energy selective spectroscopy (EELS) and energy selective imaging (ESI), HAADF STEM facility, EDS probe for chemical analysis, integrated tomographic HW and SW. The samples were dispersed by sonication in a 1:1 solvent mixture of isopropanol/ CHCl_3 and a drop of the obtained solution was deposited on a holey-carbon film supported on a copper TEM grid of 300 mesh. Histograms of the particle size distribution were obtained by counting at least 500 particles. The mean particle diameter (d_m) was calculated by using the formula $d_m = \frac{\sum d_i n_i}{\sum n_i}$, where n_i is the number of particles with diameter d_i .

Inductively coupled plasma-optical emission spectrometry (ICP-OES) was carried out with an iCAP 6200 Duo upgrade, Thermofisher instrument. A sample (0.5 mL) of Pd-solvated metal

atoms (SMA) solution was heated over a heating plate in a porcelain crucible in the presence of aqua regia (2.0 mL) for six times followed by dissolving the solid residue in 0.5 M aqueous HCl.

Powder X-ray diffraction (PXRD) experiments were carried out at room temperature with a PANalytical X'PERT PRO powder diffractometer, employing $\text{Cu K}\alpha$ ($\lambda = 1.5418 \text{ \AA}$) radiation and a parabolic MPD-mirror. Diffractograms were acquired in the 2θ range from 5.0° to 80.0°, applying a step size of 0.1050° and a counting time of 441 s.

Thermogravimetric (TG) analyses were carried out under nitrogen atmosphere using a Seiko EXSTAR 7200 TG/DTA instrument. TG spectra were collected on samples of 5–10 mg in the temperature range from 30 to 700 °C (N_2 flow = 200 mL/min) with a heating rate of 10 °C/min. The onset temperature of degradation (T_{onset}) is defined as the temperature that corresponds to a mass loss of 5%. The rate inflection temperature for the different degradation steps was extracted from derivative TG (DTG) curves.

X-ray photoelectron spectroscopy (XPS) analyses were performed in a UHV chamber equipped with an X-ray source (nonmonochromatized $\text{Mg K}\alpha$ source, 1253.6 eV) and an hemispherical analyzer by VSW mounting a 16-channel detector. The X-ray source, mounted at 54.44° with respect to the analyzer, was operated at a power of 100 W (10 kV and 10 mA). The analyzer has been equipped with a differential pumping stage in order to operate up to a pressure of 5×10^{-8} mbar. XPS spectra were measured at normal emission with a fixed pass energy of 22 eV for the high resolution Pd3d region spectra and 44 eV in the survey scans. All spectra were referenced to the C1s peak due to adventitious carbon at 284.5 eV. The inelastic background in the spectra was subtracted by means of the Shirley method [21]. Data analysis was based on a standard method for deconvolution using mixed Gaussian and Lorentzian line shapes for each component in the spectra.

Environmental scanning electron microscopy (ESEM) analyses were carried out on a FEI ESEM QUANTA 200 apparatus with a tungsten source using a gaseous secondary electron detector (GSED) with a 500 μm aperture. The images were collected with a magnification of 3000 \times , applying 6 kV, a chamber pressure of 3 Torr and a working distance of 7.0 mm.

2.2. Synthesis of end-functionalized macroligands *l*-PLA^R and *d*-PLA^R

A general synthetic procedure for the synthesis of *l*-PLA^R and *d*-PLA^R (R = 4-methyl-4'-(hydroxymethyl)-2,2'-bipyridine (BiPy), 4-(hydroxymethyl)-pyridine (Py) and benzyl (Bn)) is described as follows. In a Schlenk tube, *l*-lactide (*d*-lactide) (4.00 g, 28.00 mmol) was heated at 135 °C under a nitrogen atmosphere in the presence of $\text{Sn}(\text{Oct})_2$ (56.3 mg, 0.139 mmol) and ROH (0.400 mmol) for 3 h. Afterward, the reaction mixture was allowed to cool to room temperature and residual crystalline *l*- or *d*-lactide (ca. 1.0%), which sublimated during reaction, was removed mechanically from the Schlenk tube. The crude reaction product was then dissolved in CHCl_3 (20.0 mL) and precipitated upon addition of *n*-hexane (30.0 mL), giving an off-white solid powder, which was separated from solution by filtration, washed several times with *n*-hexane and dried by vacuum at room temperature for 12 h.

In case R = H (*i.e.* carboxylic acid end group) the synthetic protocol was modified as follows. To a two necked flask was added *l*-lactide (*d*-lactide) (2.50 g, 18.00 mmol), $\text{Sn}(\text{Oct})_2$ (90.00 mg, 0.222 mmol), water (5.00 μL , 0.270 mmol) and anhydrous toluene (20.0 mL) (*i.e.* in order to control the amount of water present in the reaction mixture). The reaction mixture was then refluxed under a nitrogen atmosphere for 24 h. Afterward, the obtained solution was cooled to room temperature causing the precipitation of a white solid. The crude product was dissolved in CH_2Cl_2 (20.0 mL), passed through a paper filter and to the clear solution

was added *n*-hexane (30.0 mL), causing the precipitation of an off-white solid which was successively separated, washed with *n*-hexane (3×10.0 mL) and dried by vacuum at room temperature for 12 h.

Yield: *l*-PLA^{BiPy} (3.70 g, 90%), *d*-PLA^{BiPy} (3.80 g, 95%); *l*-PLA^{Py} (3.80 g, 95%), *d*-PLA^{Py} (3.70 g, 93%); *l*-PLA^{Bn} (3.80 g, 96%), *d*-PLA^{Bn} (3.40 g, 90%); *l*-PLA^H (2.40 g, 96%), *d*-PLA^H (2.40 g, 96%). The molar weight of the polymers (M_n) and the poly-dispersity index (PDI) were determined by GPC, using a refraction index (RI) detector.

M_n (PDI): *l*-PLA^{BiPy}, 10,570 g/mol (1.81); *d*-PLA^{BiPy}, 10,600 g/mol (1.90); *l*-PLA^{Py}, 9615 g/mol (1.22); *d*-PLA^{Py}, 10,556 g/mol (1.37); *l*-PLA^{Bn}, 10,800 g/mol (1.62); *d*-PLA^{Bn}, 10,590 g/mol (1.90); *l*-PLA^H, 9460 g/mol (1.87); *d*-PLA^H, 8170 g/mol (1.90).

¹H NMR data for *l/d*-PLA^{Py} [22] and *l/d*-PLA^{Bn} [23] correspond to those reported in the literature.

NMR data for *l/d*-PLA^{BiPy}: ¹H (300.13 MHz, CDCl₃, ppm) = δ 1.58 (d, ³J_{HH} = 7.0 Hz, 442H, CH₃), 2.47 (s, 3H, BiPyCH₃CH₂O), 4.38 (q, ³J_{HH} = 7.0 Hz, 1H, CH(terminal)), 5.17 (q, ³J_{HH} = 7.0 Hz, 147H, CH), 5.26 (s, 2H, BiPyCH₃CH₂O), 7.18 (br. s. 1H, ArH), 7.28 (1H, ArH, overlapped with CHCl₃), 8.25 (s, 1H, ArH), 8.35 (s, 1H, ArH), 8.57 (br. s. 1H, ArH), 8.70 (br. s. 1H, ArH). ¹³C{¹H} (100.62 MHz, CDCl₃, ppm) = δ 16.64 (s, CH₃), 20.52 (s, CH₃(terminal)), 21.20 (s, BiPyCH₃CH₂O), 65.37 (s, BiPyCH₃CH₂O), 66.71 (s, CH(terminal)), 69.01 (s, CH), 119.42 (s, ArC), 121.70 (s, ArC), 122.07 (s, ArC), 125.02 (s, ArC), 145.05 (s, ArC), 149.01 (s, ArC), 149.50 (s, ArC), 169.60 (s, COOC), 175.34 (s, COOR).

NMR data for *l/d*-PLA^H: ¹H (400.13 MHz, CDCl₃, ppm) = δ 1.57 (d, ³J_{HH} = 7.1 Hz, 390H, CH₃), 4.38 (br s, 1H, CH(terminal)), 5.18 (q, ³J_{HH} = 7.1 Hz, 130H, CH). ¹³C{¹H} (100.62 MHz, CDCl₃, ppm) = δ 16.64 (s, CH₃), 20.26 (s, CH₃(terminal)), 65.85 (s, CH (terminal)), 66.72 (s, CH(terminal)), 69.01 (s, CH), 169.61 (s, COOC), 172.98 (s, COOH), 175,15 (s, COOC(terminal)).

2.3. Synthesis of the stereocomplexes L^R

Solutions of *l*-PLA^R and *d*-PLA^R (800.0 mg) in CH₂Cl₂ (8.0 mL) with identical R, were mixed at room temperature under vigorous stirring for half an hour. Afterward the obtained clear solution was concentrated to dryness by means of a vacuum pump at room temperature. The obtained off-white solids were used without further purification. Yield: 90–95%.

2.4. Synthesis of supported Pd-NPs Pd@L^R and Pd@C by MVS technique

In a typical synthesis procedure, Pd vapor generated at 1.5×10^{-6} psi by resistive heating of the metal (500.0 mg) in an alumina-coated tungsten crucible was co-condensed with a 1:1 mixture of mesitylene (30.0 mL) and 1-hexene (30.0 mL) in a glass reactor at liquid nitrogen temperature. The reactor chamber was heated to the melting point of the solid matrix (ca. -40 °C), and the resulting brown solution was siphoned and handled at low temperature (-20 °C) with the Schlenk tube technique. The Pd-content of the obtained Pd solvated metal atoms (SMA) determined by ICP–OES analysis was 1.4 mg of Pd/mL. In a Schlenk tube a portion of the Pd SMA (3.0 mg, 2.2 mL) was added to L^R (500.0 mg) or Vulcan XC-72 (C) in deaerated CHCl₃ (10.0 mL) under nitrogen atmosphere and the resulting suspension was allowed to stir at 25 °C for 6 h. The addition of an excess of diethyl ether (50.0 mL) to the latter solutions caused the precipitation of a gray (Pd@L^R) or black (Pd@C) powder, which was isolated upon centrifugation of the suspension and successive decanting of the colorless supernatant. The obtained powder was dried under reduced pressure. All isolated samples contained 0.6 w/w% of Pd as determined by ICP–OES analysis. The sample containing a 3.0 w/w% Pd loading (Pd@L^{BiPy}) was prepared by applying the

same synthesis procedure as reported above and by using 10.7 mL of Pd SMA (15.9 mg).

2.5. Synthesis of Pd(OAc)₂(*d*-PLA^{BiPy})

To a solution of *d*-PLA^{BiPy} (300.0 mg, 0.0284 mmol) in CH₂Cl₂ (10.0 mL) was added Pd(OAc)₂ (OAc = acetate) (6.46 mg, 0.0288 mmol) and the resulting solution was stirred under a nitrogen atmosphere at room temperature for 6 h. Afterward the solvent was removed completely by vacuum and the slightly yellow solid was washed with diethyl ether (2×5.0 mL). Yield: 275.6 mg, 90%. ¹H NMR (300.13 MHz, CD₂Cl₂, ppm) = δ 1.58 (d, ³J_{HH} = 7.0 Hz, 442H, CH₃), 2.01 (br s, 6H, OAc), 2.53 (s, 3H, BiPyCH₃CH₂O), 4.38 (q, ³J_{HH} = 7.0 Hz, 1H, CH(terminal)), 5.19 (q, ³J_{HH} = 7.0 Hz, 147H, CH), 5.24 (s, 2H, BiPyCH₃CH₂O), 7.31 (br. s. 1H, ArH), 7.38 (br. s, 1H, ArH), 7.90 (br s, 2H, ArH), 8.22 (br. s. 1H, ArH), 8.39 (br. s. 1H, ArH).

2.6. Reduction of Pd(OAc)₂(*d*-PLA^{BiPy}) and *trans*-[Pd(OAc)₂(*d*-PLA^{Py})₂] with hydrogen

Deaerated solutions of Pd(OAc)₂(*d*-PLA^{BiPy}) and *trans*-[Pd(OAc)₂(*d*-PLA^{Py})₂] [24] (300.0 mg) in CH₂Cl₂ (7.0 ml) were transferred to Teflon-coated stainless steel autoclaves (80.0 mL) which were sealed and pressurized with hydrogen (15.0 bar). The autoclaves were then stirred for 12 h at room temperature, followed by releasing the excess hydrogen and transferring the black solutions to round-bottom flasks. The solvent was in both cases completely evaporated, and the dark brown solids were washed with diethyl ether (2×5.0 mL) and vacuum-dried. Yield: 85–90%.

2.7. Catalytic cinnamaldehyde hydrogenation reactions

2.7.1. Hydrogenation reactions in THF solution

Pd@L^R (21.0 mg, 0.0012 mmol Pd) was added to a Teflon-coated stainless steel autoclave (80.0 mL) equipped with magnetic stirrer, temperature and pressure controller, which was sealed and evacuated. A solution of cinnamaldehyde (141.0 μ L, 1.12 mmol) in deaerated THF (10.0 mL) was introduced in the autoclave by suction. Then the autoclave was placed into a stirred oil bath which was heated to 60 °C. Once the latter temperature was reached, the autoclave was pressurized with hydrogen (150 psi) and stirred at 700 rpm for the stabilized reaction time. The autoclave was then successively cooled to 10 °C by a water/ice bath, the hydrogen gas vented off and the heterogeneous catalyst separated from THF solution by decantation. The solid catalyst was washed with fresh THF (5.0 mL) and the combined THF solutions were analyzed by GC and GC–MS. Recycling experiments were carried out with the latter recovered, THF-washed and vacuum-dried catalyst following the same experimental procedure as described above.

2.7.2. Solventless hydrogenation reactions

Pd@L^{BiPy} (40.0 mg, 0.014 mmol, 3.0 w/w% Pd loading) was placed into a Teflon-coated stainless steel autoclave (80.0 mL) together with the substrate (3.0 mL, 24.0 mmol). The autoclave was then sealed and flushed with nitrogen for 2 min. Afterward the autoclave was pressurized with hydrogen gas, heated at 60 °C by means of an oil bath and stirred at 700 rpm. The autoclave was continuously fed with hydrogen gas from a reservoir in order to maintain a constant gas pressure (150 psi) during the catalytic reaction. After the desired reaction time, the autoclave was cooled to room temperature and the excess of hydrogen vented off. To the dark suspension was added diethyl ether (8.0 mL) causing the separation of the catalyst, which settled at the bottom of the autoclave. The supernatant was decanted and the catalyst was

washed with diethyl ether (2×3.0 mL). The combined diethyl ether phases were analyzed by GC.

3. Results and discussion

3.1. Synthesis and characterization of end-functionalized stereocomplexes

PLA containing a functional end-group R (*l/d*-PLA^R) with R = 4-methyl, 4-methylene-2,2'-bipyridine (BiPy), 4-methylenepyridine (Py) and benzyl (Bn) attached covalently via an ester group to the polymer backbone was synthesized by Sn(Oct)₂-catalyzed ring opening polymerization (ROP) [23] of bulk *l*- and *d*-lactide in the presence of the polymerization initiator ROH (Scheme 1) at 135 °C. In contrast, carboxylic acid end-functionalized *l*-PLA and *d*-PLA (*i.e.* *l*-PLA and *d*-PLA^H) were obtained upon the same catalytic reaction carried out in refluxing toluene instead of molten lactide and in the presence of a defined amount of water as polymerization initiator. The end-functionalized polymers obtained were white solids, featured by a molar weight (M_n) in the range between 9000 and 11,000 g/mol (*i.e.* determined by GPC in THF) which corresponds to a polymerization degree of 125–150, due to the chosen molar ratio between lactide and the polymerization initiator ROH of 70. XPS analyses of L^R proved the presence of Sn(II) (*i.e.* binding energy for Sn3d_{5/2} of 486.5 eV) on the polymer surface, which stems from the Sn-catalyst used for the ROP [25].

PXRD spectra showed a typical diffraction pattern of crystalline PLA (Fig. S1), while the successful incorporation of the functional groups (R) in the PLA backbone was proved by acquiring ¹³C{¹H} NMR spectra in CDCl₃ showing for R = Bn, Py and BiPy a singlet at ca. 65.4 ppm which corresponds to the methylene unit of the functional groups attached *via* ester functionality to PLA, whereas, a broad ¹³C{¹H} NMR singlet centered at 172.97 ppm for *l/d*-PLA^H proved the presence of a carboxylic acid terminal group in the latter polymer [26].

Equimolar solutions of *l*- and *d*-PLA^R in CH₂CH₂ with identical R were mixed at room temperature, obtaining a clear solution which upon solvent evaporation gave the corresponding stereocomplex L^R [14] (Scheme 1) as an off white solid in 90–95% yield.

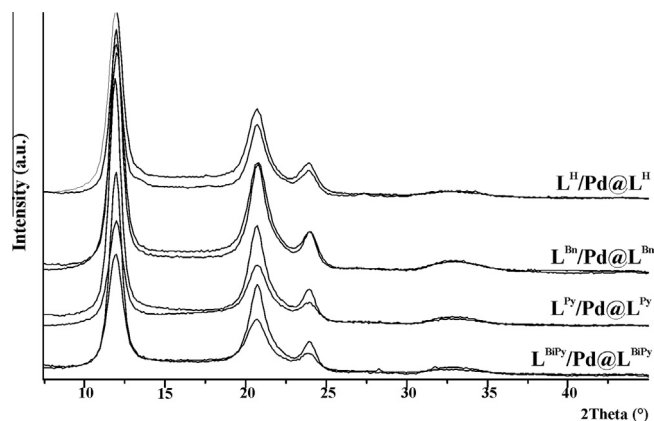
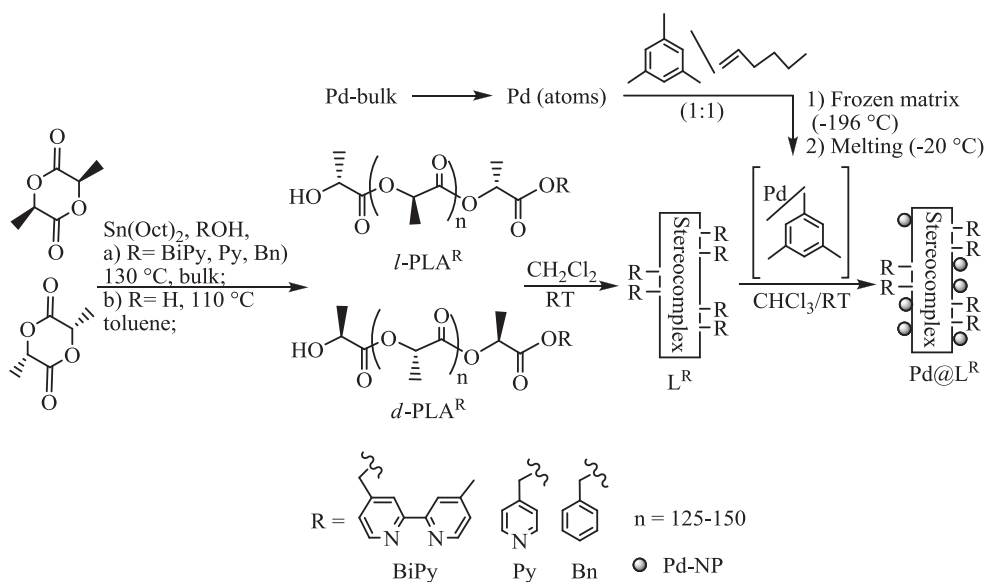


Fig. 1. PXRD diffractograms of L^R (upper traces) and Pd@L^R.

Room temperature PXRD spectra of L^R exhibited the characteristic Bragg reflexes of the PLA-stereocomplex L centered at 12.048°, 20.783°, 23.982° and 32.781° (2θ) [27,28] regardless of the nature of terminal group present in the PLA backbone (Fig. 1, upper traces).

The thermal stability of L^R was studied by TG analyses carried out under a nitrogen atmosphere. As a result L^{BiPy/Py/Bn} showed a T_{onset} (*i.e.* temperature at 5% weight loss) between 259.9 and 239.7 °C, whereas L^H (*i.e.* carboxylic acid polymer termination) exhibited the lowest T_{onset} of 214.5 °C. This experimental result clearly indicates an increase of the thermal stability of the polyester-based polymer when the polymer chain ends with an ester functionality instead of a carboxylic acid group. The former functional group notably retards the back-biting of terminal lactate unit, shortening hence the polymer chain under the concomitant release of lactide [14].

ESEM micrographs acquired for L^{BiPy/Py/Bn/H} under identical experimental conditions (*i.e.* magnification of 3000 \times , working distance of 6.9 mm) showed for L^H a significantly rougher surface compared to L^{BiPy/Py/Bn} (Fig. S2). In fact, a similar surface roughness was observed after hydrolytic degradation of PLA characterized by a terminal ester functionality [16].



Scheme 1. Synthesis of *l/d*-PLA^R, L^R and Pd@L^R.

3.2. Synthesis and characterization of Pd-NPs onto end-functionalized stereocomplexes

Pd-NPs supported onto L^R were obtained by means of the MVS technique [12,18,19]. According to this latter synthesis approach a Pd-vapor was co-condensed with vapors of mesitylene and 1-hexene at -196°C . Upon warming of the latter matrix to -20°C , a brown solution of Pd-solvated atoms was obtained to which was added L^R dispersed in CHCl_3 (Scheme 1). The L^R supported Pd-NPs (*i.e.* $\text{Pd}@L^R$) were isolated upon addition of diethyl ether, causing the precipitation of $\text{Pd}@L^R$ as a gray powder

which was dried under vacuum. The Pd-content of $\text{Pd}@L^R$, determined by ICP-OES, was 0.6 w/w%.

Isolated samples of $\text{Pd}@L^R$ were analyzed by HRTEM, PXRD, XPS, IR spectroscopy and TGA. HRTEM micrographs of $\text{Pd}@L^{\text{BiPy}}$ and $\text{Pd}@L^{\text{Py}}$ (Fig. 2) showed well-dispersed NPs characterized by the same average size (d_m) of 2.0 ± 0.6 nm.

In contrast, HRTEM micrographs of $\text{Pd}@L^{\text{Bn/H}}$ (Fig. 3) exhibited Pd-NPs of comparable size, which formed large aggregates, leading hence to a poor Pd dispersion on the polymer surface. In fact, bipyridine and pyridine end-functionalized polymers revealed notable Pd-NP stabilizing properties [13,19,24,29,30]. Even on

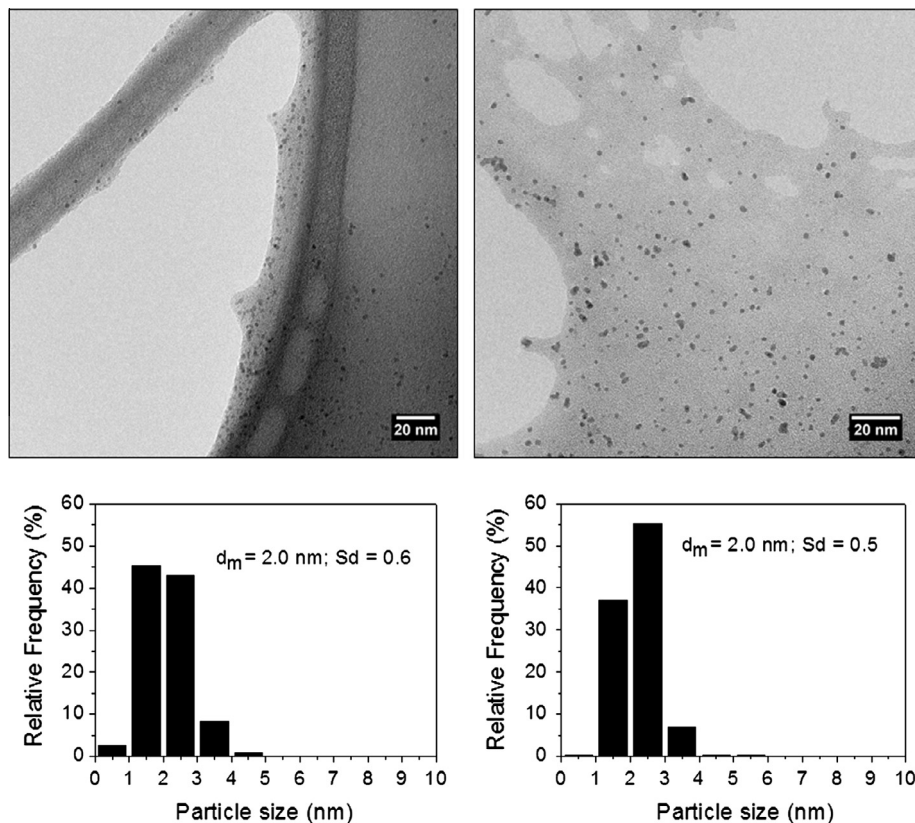


Fig. 2. HRTEM micrographs and histograms of $\text{Pd}@L^{\text{BiPy}}$ (left) and $\text{Pd}@L^{\text{Py}}$ (right).

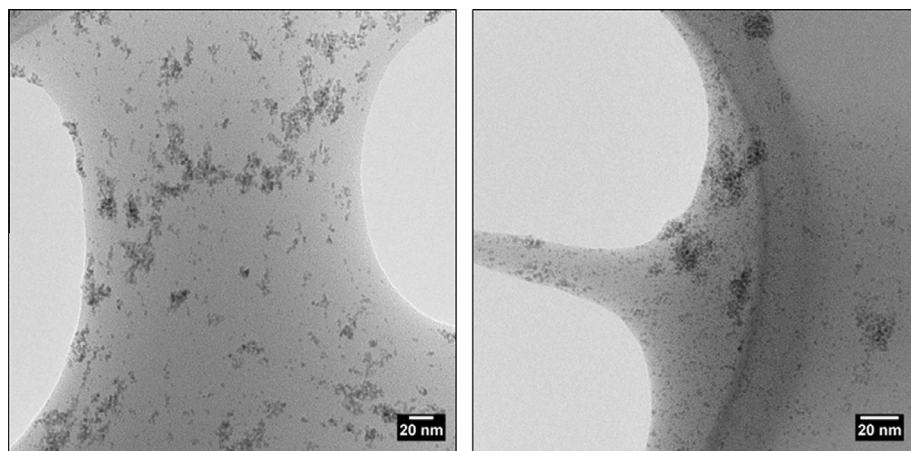


Fig. 3. HRTEM micrographs of $\text{Pd}@L^{\text{Bn}}$ (left) and $\text{Pd}@L^{\text{H}}$ (right).

increasing the Pd loading from 0.6 to 3.0 w/w% as in Pd@L^{BiPy}, a similar Pd dispersion was obtained (i.e. Pd-NPs of 2.3 ± 0.7 nm, Fig. S3).

PXRD spectra of Pd@L^R (Fig. 1, lower traces) showed in all cases the same diffraction pattern as for the polymer support (L^R) proving that no alteration of the support occurred in the course of the Pd-NP generation by MVS technique.

XPS analysis of Pd@L^R showed the presence of Pd(0) (65%) and Pd(II) (35%) regardless of the polymer support employed. The rather small Pd-NPs found in Pd@L^R are reactive and can hence be easily be oxidized to PdO even under a careful treatment of the Pd-NP sample after MVS (i.e. samples stored under nitrogen atmosphere). In fact, the Pd(0)/Pd(II) molar ration found is in accordance with Pd-NPs covered by a monolayer of PdO [31,32].

A comparison of the ATR-IR spectra of L^{BiPy/H} with those of Pd@L^{BiPy/H} showed at a first glance the typical IR absorption bands of the PLA stereocomplex (Fig. S5) [33]. However, in case of L^{BiPy} we observed the characteristic H-out of plane bending motion of 2,2'-bipyridine at 738 cm^{-1} [34] (Fig. 4, trace c, peak labeled with asterisk), while the one at 757 cm^{-1} was overlapped by a bending motion of PLA [33]. In contrast, Pd@L^{BiPy} (Fig. 4, trace d) showed the absence of the absorption band at 738 cm^{-1} , which might be the result of interactions of the aromatic rings of 2,2'-bipyridine with the Pd-NPs' surface. To verify this hypothesis, we reduced the model compound Pd(OAc)₂(2,2'-bipyridine) (OAc = acetate) [35] with hydrogen pressure to 2,2'-bipyridine stabilized Pd-NPs. As a result, the IR spectrum of 2,2'-bipyridine-stabilized Pd-NPs showed a notable intensity decrease of the absorption band at 757 and 738 cm^{-1} (Fig. S6).

TG analyses carried out on Pd@L^{BiPy/Py/Bn/H} in an nitrogen atmosphere clearly showed an increased thermal stability of the functionalized stereocomplexes in the presence of Pd-NPs. Accordingly, the T_{onset} of degradation of the polymer structure of Pd@L^{BiPy/Py/Bn/H} shifted to higher values compared to L^{BiPy/Py/Bn/H} (i.e. 273.9 vs $259.9\text{ }^{\circ}\text{C}$ (L^{BiPy}), 285.6 vs $250.5\text{ }^{\circ}\text{C}$ (L^{Py}), 272.3 vs $239.7\text{ }^{\circ}\text{C}$ (L^{Bn}) and 232.5 vs $214.5\text{ }^{\circ}\text{C}$ (L^H)). It is furthermore important to stress on the fact that L^R decompose upon melting (ca. $225\text{ }^{\circ}\text{C}$), regardless of the nature of the terminal group. The presence of Pd-NPs onto L^{BiPy/Py/Bn} led to recrystallization of the

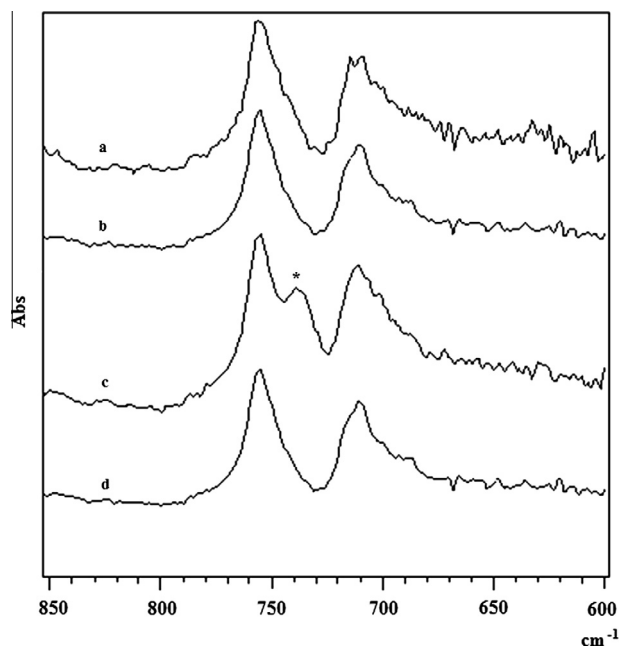


Fig. 4. ATR-IR spectra of L^H (a), Pd@L^H (b), L^{BiPy} (c) and Pd@L^{BiPy} (d).

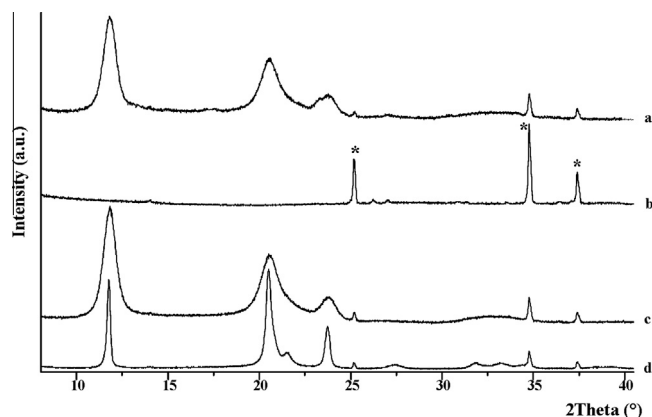


Fig. 5. PXRD spectra acquired at room temperature of: Pd@L^H as-synthesized (a); after melting and cooling to room temperature (b); Pd@L^{BiPy} as-synthesized (c) and after melting and cooling to room temperature (d). Bragg reflexes labeled with an asterisk are assigned to the sample holder material (Al₂O₃).

polymer upon cooling of the melt, as shown by PXRD for Pd@L^{BiPy} (Fig. 5, trace d vs c). A similar enhanced thermal stability of polystyrene and polypropylene in the presence of Pd-NPs was rationalized by a reduced mobility of the polymer chains in the presence of NPs, avoiding the intermolecular free radical transfer [36]. In contrast Pd@L^H decomposed upon melting. Accordingly, after melting and cooling of Pd@L^H only Bragg reflexes stemming from sample holder material (Fig. 5, trace b) were observed.

3.3. Catalytic hydrogenation reactions

The catalysts Pd@L^{BiPy/Py/Bn/H} were employed to hydrogenate cinnamaldehyde which is a structure sensitive model compound for α,β -unsaturated carbonyl compounds in THF at $60\text{ }^{\circ}\text{C}$. The catalysts are completely insoluble in THF [13].

Hydrogen pressure (150 psi) and stirring rate (700 rpm) were chosen to guarantee a substrate conversion without notable mass-transport effects. Pd@C (i.e. C = Vulcan XC-72 (254 m²/g), Pd loading of 0.6 w/w% and NPs size of 2.6 ± 0.7 nm (Fig. S4)) were chosen as catalytic reference system. The metal dispersion for Pd@L^{BiPy/Py} (0.6 w/w% Pd loading), Pd@L^{BiPy} (3.0 w/w% Pd loading) and Pd@C (0.6 w/w% Pd loading) was calculated from HRTEM data applying the equation: $d_{\text{VS}}/d_{\text{at}} = 3.32/(\text{FE})^{1.23}$ with d_{VS} = mean size of Pd crystallites, d_{at} = atomic diameter of Pd (0.275 nm) and FE the exposed fraction of Pd [37]. As a result, Pd@L^{BiPy/Py} and Pd@C exhibited a metal dispersion of 53% and 43%, respectively. The results obtained from the catalysts' screening are compiled in Table 1 and normalized TOF values are reported only for Pd@L^{BiPy/Py} which showed uniformly dispersed Pd-NPs.

A blank reaction conducted with L^{BiPy} under catalytic conditions reported in Table 1 for 2 h gave a substrate conversion of 1.4%, which is indicating a negligible contribution of tin residues (i.e. stemming from ROP of lactide) to the observed catalytic activity of Pd@L^R.

A comparison of the catalytic performance of Pd@L^R showed under identical catalytic conditions the following trend of activity: Pd@L^{BiPy} > Pd@L^{Py} > Pd@L^{Bn} > Pd@L^H. The much higher catalytic activity of Pd@L^{BiPy/Py} compared to Pd@L^{Bn/H} is due to the higher Pd-dispersion found for the former catalysts, as proved by the corresponding TEM-images acquired for the as-synthesized catalysts (Figs. 2 and 3). Consequently, more substrate accessible metal sites on the NP surface are available for the catalytic hydrogenation reaction. The chemoselectivity for C=C bond hydrogenation of cinnamaldehyde to give 3-phenylpropanal followed the same trend as observed for the catalytic activity, showing for Pd@L^{BiPy} a

Table 1
Hydrogenation of cinnamaldehyde by Pd@C, Pd@L^{BiPy}/Py/Bn/H and Pd'@L^{BiPy}.

Entry ^a	Catalyst	t (h)	Conv.(%)/TOF (h ⁻¹) ^b	Sel.(%) ^c
1	Pd@L ^{BiPy}	1	38/682	99
2	Pd@L ^{BiPy}	2	74/664	97
3	Pd@L ^{BiPy}	3	100/n.d.	95
4 ^d	Pd@L ^{BiPy}	2	72/646	96
5 ^e	Pd@L ^{BiPy}	2	69/619	94
6 ^f	Pd'@L ^{BiPy}	2	65/645	95
7 ^{d,f}	Pd'@L ^{BiPy}	2	55/n.d.	90
8	Pd@L ^{Py}	2	54/485	88
9 ^d	Pd@L ^{Py}	2	42/377	75
10 ^e	Pd@L ^{Py}	2	30/269	68
11	Pd@L ^{Bn}	2	30/n.d.	65
12	Pd@L ^H	2	14/n.d.	60
13	Pd@C	2	99/921	55
<i>Solventless hydrogenation^g</i>				
14	Pd'@L ^{BiPy}	2	30/547	95
15	Pd'@L ^{BiPy}	4	58/n.d.	91
16	Pd'@L ^{BiPy}	6	88/n.d.	90

^a Catalytic conditions: Pd (0.0012 mmol), cinnamaldehyde (141.2 μL, 1.12 mmol), THF (10.0 mL), p(H₂) = 150 psi, T = 60 °C.

^b Normalized TOF (i.e. mmol substrate (converted) × (mmol Pd_(surface))⁻¹ × h).

^c Selectivity for 3-phenylpropanal.

^d 2nd recycling experiment.

^e 4th recycling experiment.

^f The same amount of Pd exposed as Pd@L^{BiPy}.

^g Pd' (3.0 w/w% metal loading, 0.014 mmol), cinnamaldehyde (3.0 mL, 24.0 mmol).

chemoselectivity of 99% (Table 1, entry 1), which decreased to 95% at complete substrate conversion (Table 1, entry 3). This latter chemoselectivity is significantly higher compared to that observed for Pd@C (55%) at the same substrate conversion (Table 1, entry 3 vs 13).

Pd@L^{Bn/H} which is characterized by the presence of NPs-aggregates on the polymer surface showed much higher C=O hydrogenation activity compared to Pd@L^{BiPy/Py}. This latter experimental fact corroborates the known observation that the formation of cinnamyl alcohol is strictly related to the shape of the Pd-NP surface. Large particles, which have a small surface curvature trigger the repulsion of the phenyl ring from the metal surface [38,39]. As a consequence, the interaction of C=O is favored over C=C with the NP surface, fostering hence the hydrogenation of the C=O bond.

Interestingly, on varying the molar ratio between the anchored bipyridine functionalities and the surface Pd atoms (i.e. Pd@L^{BiPy}: BiPy to Pd_{surface} of 6 vs Pd'@L^{BiPy}: BiPy to Pd_{surface} of 0.7) the chemoselectivity was notably altered, even when the initial particle size was comparable (i.e. 2.0 nm (Pd@L^{BiPy}) and 2.3 nm (Pd'@L^{BiPy})). As a result, Pd'@L^{BiPy} exhibited under identical experimental conditions a chemoselectivity and substrate conversion which was lower compared to Pd@L^{BiPy} (Table 1, entry 6 vs 2). In addition, a recycling experiment with Pd'@L^{BiPy} clearly confirmed a drop of chemoselectivity to 90% (Table 1, entry 7 vs 6), which is a direct consequence of the scarce stabilization of the initially small NPs, in case of an almost 1:1 M ratio between 2,2'-bipyridine functional groups and surface Pd atoms [40–42].

Recycling experiments with Pd@L^{BiPy/Py} were carried out, recovering the catalyst by a simple filtration and washing with THF in air atmosphere. Pd@L^{BiPy} showed a comparable catalytic performance in the different recycling experiments (Table 1, entry 2 vs 4 and 5). In contrast, Pd@L^{Py} exhibited a significant drop of catalytic activity as well as chemoselectivity (i.e. from 88% to 68% after the fourth catalytic cycle) (Table 1, entry 8 vs 9 and 10).

We tested the catalytic performance of Pd'@L^{BiPy} also under solventless catalytic conditions (Table 1, entries 14–16) applying

a substrate to Pd molar ratio of 1714. Since the hydrogenation of 3.0 mL of cinnamaldehyde consumed a notable amount of hydrogen, the autoclave was continuously fed with hydrogen from a reservoir in order to guarantee a constant gas pressure in the course of the catalytic reactions. The substrate conversion reached 88% after a reaction time of 6 h, along with a chemoselectivity of 90%.

3.4. Analysis of recovered catalysts

Pd@L^{BiPy/Py} was easily recovered from catalytic reactions carried out in THF by simply decanting the supernatant and washing the solid with THF. Pd'@L^{BiPy} was recovered from solventless catalytic reactions by adding diethyl ether to the reaction mixture, causing the separation of the polymer from organic substrate. The supernatant was then simply decanted and the catalyst washed with diethyl ether. ICP-OES analysis of the catalytic THF solutions stemming from Pd@L^{BiPy}-catalyzed reactions showed the presence of a very low amount of Pd (i.e. <0.5 ppm), confirming an efficient anchoring of Pd on the polymer support.

HRTEM micrographs obtained from recovered Pd@L^{BiPy/Py} after hydrogenation of cinnamaldehyde for 2 h (Fig. 6) showed a slight increase of the particle size in both cases compared to the corresponding as-synthesized catalysts (i.e. 2.8 ± 0.7 (Pd@L^{BiPy}) and 3.1 ± 0.8 nm (Pd@L^{Py}) vs 2.0 ± 0.5 nm (as-synthesized catalysts)). STEM images of both latter recovered catalysts (Fig. 6) clearly exhibited a much more pronounced Pd-NP aggregation for Pd@L^{Py}, which is in accordance with a significantly higher drop of the catalytic activity and chemoselectivity found for Pd@L^{Py} compared to Pd@L^{BiPy}.

PXRD spectra of Pd'@L^{BiPy}, recovered after solventless catalytic reactions conducted at different reaction times showed for the support the same diffraction pattern as the as-synthesized catalyst (Fig. S7) proving the stability of the support even under non-diluted catalytic conditions. A slow acquisition of the same spectra in the 2θ range between 36.5° and 42.5° (Fig. 7) exhibited an intensity change of the characteristic 111 Bragg reflex of fcc Pd centered at ca. 39.0° (2θ). As a result, the Pd-NP size, determined by the Debye–Scherrer method [43] using the Pd (111) Bragg reflex, increased during the first 2 h from 2.0 to 3.9 nm, whereas the Pd-NP size detected after 4 h is almost identical to that after 2 h.

XPS spectra acquired in the Pd3d region for recovered Pd'@L^{BiPy} after a solventless hydrogenation reaction lasting 2 h (Fig. 8) showed 69.4% Pd(0) (i.e. Pd 3d_{5/2}, 334.8 eV and Pd 3d_{3/2}, 340.6 eV) [44] and 30.6% Pd(II) (i.e. Pd 3d_{5/2}, 337.2 eV and Pd 3d_{3/2}, 342.4 eV) [45] on the NPs' surface, which is similar to those observed for the as-synthesized catalyst (i.e. 68.4% Pd(0) and 31.6% Pd(II)). This experimental result is rationalized by a fast re-oxidation of Pd(0) located at the Pd-NP surface to PdO [31].

In order to underscore the significantly higher Pd-NP-stabilizing properties of 2,2'-bipyridine compared to pyridine, we synthesized the model Pd(OAc)₂-macrocomplexes (OAc = acetate) of the formula Pd(OAc)₂(d-PLA^{BiPy}) and trans-[Pd(OAc)₂(d-PLA^{Py})₂] [24] (Scheme 2) which share the same nitrogen to Pd atom ratio.

Upon reduction of CH₂Cl₂ solutions of the latter Pd-macrocomplexes by means of hydrogen, d-PLA^{BiPy} and d-PLA^{Py}-stabilized Pd-NPs were obtained and analyzed by TEM measurements. As a result, only Pd@d-PLA^{BiPy} showed well-dispersed Pd-NPs with an average size of 3.8 ± 0.6 nm (Fig. S14), while Pd@d-PLA^{Py} exhibited worm-like structures of Pd-NP aggregates, which resembled those obtained after the reduction of trans-[Pd(OAc)₂(PEG^{Py})₂] (PEG = poly(ethyleneglycol)) under identical experimental conditions [24]. Pd@PLA^{BiPy} is characterized by a Pd content of 1.0 wt% and a molar ratio between 2,2'-bipyridine units and surface Pd atoms of 3. A parallel catalytic reaction with

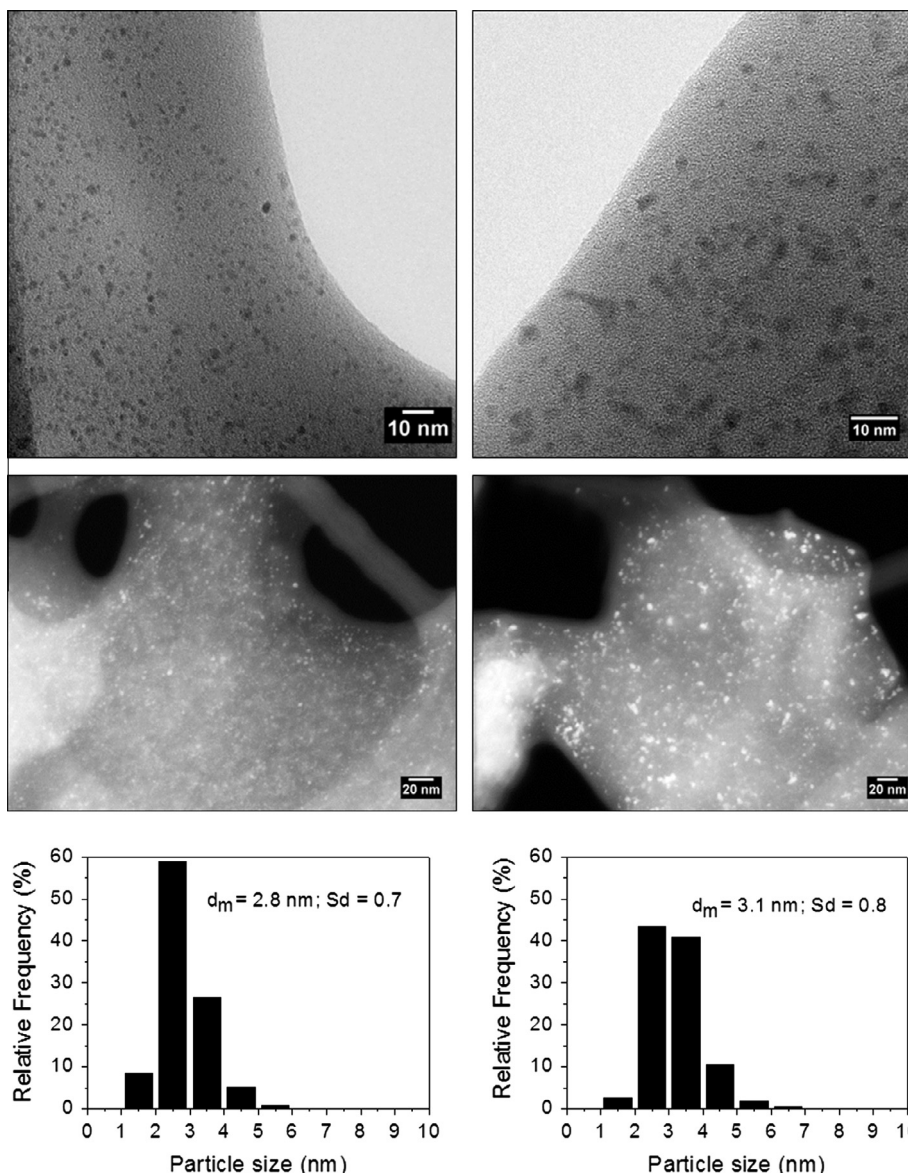


Fig. 6. HRTEM (upper) and HRSTEM (middle) micrographs and histograms of recovered Pd@L^{BiPy} (left) and Pd@L^{Py} (right) after catalysis conducted at 60 °C.

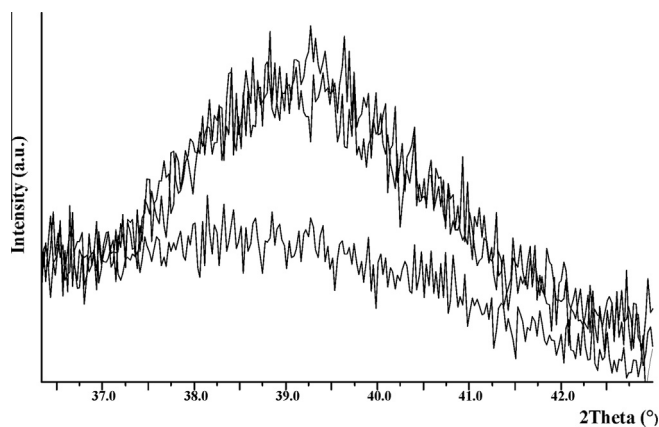


Fig. 7. PXRD diffractograms of Pd@L^{BiPy} acquired between 36.5° and 42.5° (2 θ): as-synthesized (lower trace); after solventless catalysis conducted for 2 h and 4 h (upper traces).

Pd@*d*-PLA^{BiPy} under experimental conditions identical to that reported in Table 1, gave a chemoselectivity for 3-phenylpropanal of 91% along with a substrate conversion of 57% for a reaction time of 2 h. This experimental result corroborates again the drop of chemoselectivity for 3-phenylpropanal by increasing the size of the Pd-NP.

Based on experimental data stemming from TEM, XPS and IR-measurements along with catalytic data collected for Pd@L^{BiPy}, we propose the following catalytic cycle operative for the Pd@L^{BiPy}-catalyzed cinnamaldehyde hydrogenation as sketched in Fig. 9.

Upon the reaction of the as-synthesized Pd-NPs of Pd@L^{BiPy} the oxide layer is removed and the naked Pd-surface activates hydrogen that reacts with the C=C coordinated cinnamaldehyde to give 3-phenylpropanal. Anchored 2,2'-bipyridine controls catalytic activity and the size of the Pd-NPs by reversible discoordination (i.e. making accessible catalytically active sites) and coordination to the surface Pd atoms [42].

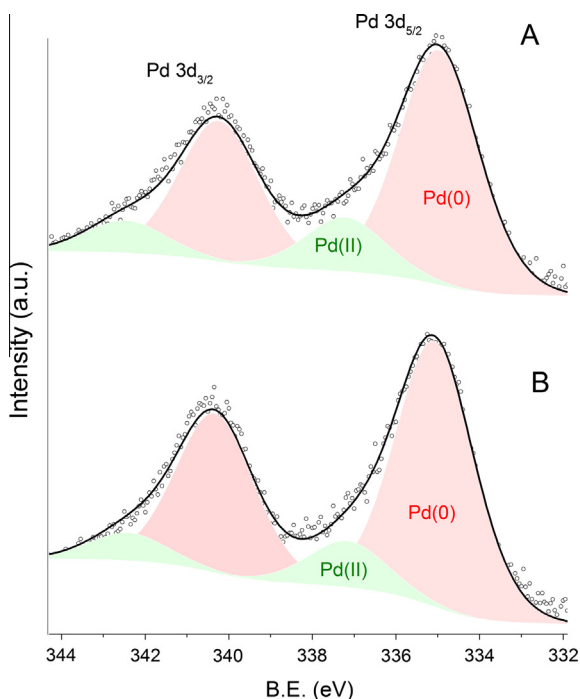
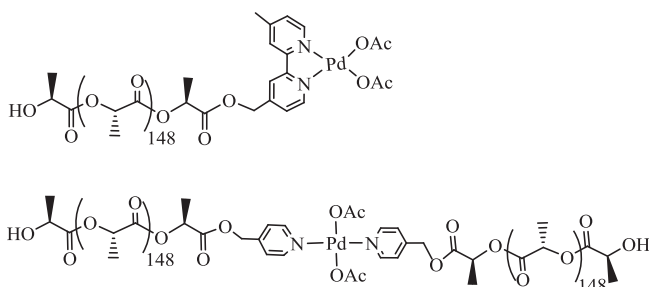


Fig. 8. Pd3d XPS spectra of Pd@L^{BiPy} before (A) and after (2 h) solventless catalysis (B).



Scheme 2. Pd(OAc)₂-macrocomplexes with *d*-PLA^{BiPy} and *d*-PLA^{Py}.

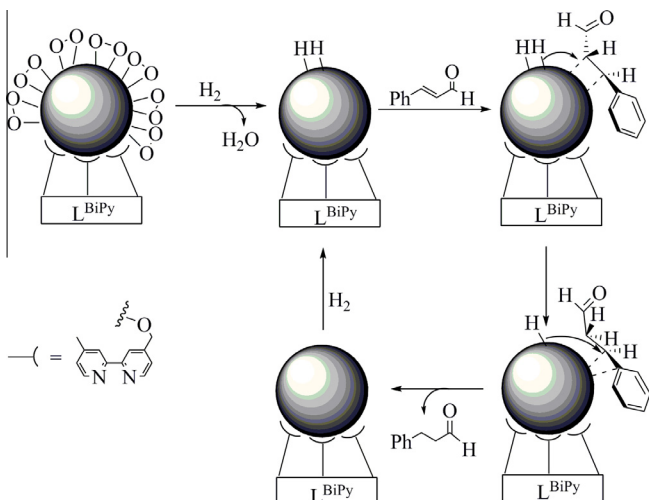


Fig. 9. Proposed catalytic cycle operative for Pd@L^{BiPy}-catalyzed cinnamaldehyde hydrogenation.

4. Conclusions

Poly(lactic acid) (PLA)-based stereocomplexes functionalized at the carboxylic acid end were used to support Pd nanoparticles (NPs), obtained by means of the metal vapor synthesis technique. The nature of the functional end group notably influenced the dispersion of Pd-NPs on the polymer support. Pd-NPs supported onto 2,2'-bipyridine end-functionalized PLA-stereocomplex (*i.e.* Pd@L^{BiPy}) exhibited the best chemoselectivity for the C=C bond reduction in cinnamaldehyde (*i.e.* 95% at complete substrate conversion). In contrast, other heterogeneous polymer-based Pd-catalysts showed significantly lower chemoselectivity for 3-phenylpropanal (*i.e.* <90%) [11,12]. The role of the polymer-anchored 2,2'-bipyridine is best described as an efficient Pd-NP stabilizer in the course of the catalytic hydrogenation reaction, provided the molar ratio between the 2,2'-bipyridine units and the Pd surface is high enough. Indeed, when the latter ratio was 6, as found for Pd@L^{BiPy}, small Pd-NPs of 2.0 nm were efficiently stabilized. Consequently, the high chemoselectivity observed for 3-phenylpropanal with Pd@L^{BiPy} is particle size driven [46,47] (*i.e.* small particle sizes foster C=C bond coordination to the Pd surface and hence formation of 3-phenylpropanal). L^{BiPy} stabilized Pd-NPs were found robust enough to be used as recyclable catalyst.

Acknowledgments

C.E. and R.P.J. thank MIUR-Italy (FIRB 2010; contract RBF10BF5V) for financial support. Ente Cassa di Risparmio di Firenze is acknowledged for financial support and B. Cortigiani of the CeTeCS center for the technical assistance during XPS measurements.

Appendix A. Supplementary material

Supplementary data associated with this article can be found, in the online version, at <http://dx.doi.org/10.1016/j.jcat.2015.07.012>.

References

- [1] B. Chen, U. Dingerdissen, J.G.E. Krauter, H.G.J. Lansink Rotgerink, K. Möbus, D.J. Ostgard, P. Panster, T.H. Riermeier, S. Seebald, T. Tacke, H. Trauthwein, *Appl. Catal. A: Gen.* 280 (2005) 17–46.
- [2] H.U. Blaser, C. Malan, B. Pugin, F. Spindler, H. Steiner, M. Studer, *Adv. Synth. Catal.* 345 (2003) 103–151.
- [3] O.S. Chambyal, S. Paul, T. Shamim, M. Gupta, R. Gupta, A. Loupy, *Synth. Commun.* 43 (2013) 656–667.
- [4] P. Gallezot, D. Richard, *Catal. Rev. Sci. Eng.* 40 (1998) 81–126.
- [5] X. Ji, X. Niu, B. Li, Q. Han, F. Yuan, F. Zaera, Y. Zhu, H. Fu, *ChemCatChem* 6 (2014) 3246–3253.
- [6] M. Steffan, F. Klasovsky, J. Arras, C. Roth, J. Radnik, H. Hofmeister, P. Claus, *Adv. Synth. Catal.* 350 (2008) 1337–1348.
- [7] P. Claus, *Top. Catal.* 5 (1998) 51–62.
- [8] F. Delbecq, P. Sautet, *J. Catal.* 152 (1995) 217–236.
- [9] P. Kaur, J.T. Hupp, S.T. Nguyen, *ACS Catal.* 1 (2011) 819–835.
- [10] M. Králik, A. Biffis, *J. Mol. Catal. A: Chem.* 177 (2001) 113–138.
- [11] Y. Gao, C.-A. Chen, H.-M. Gau, J.A. Bailey, E. Akhadov, D. Williams, H.-L. Wang, *Chem. Mater.* 20 (2008) 2839–2844.
- [12] A.M. Raspolli Galletti, L. Toniolo, C. Antonetti, C. Evangelisti, C. Forte, *Appl. Catal. A: Gen.* 447–448 (2012) 49–59.
- [13] G. Petrucci, W. Oberhauser, M. Bartoli, G. Giachi, M. Frediani, E. Passaglia, L. Capozzoli, L. Rosi, *Appl. Catal. A: Gen.* 469 (2014) 132–138.
- [14] H. Tsuji, *Macromol. Biosci.* 5 (2005) 569–597.
- [15] S. Regnell Andersson, M. Hakkarainen, S. Inkinen, A. Södergård, A.-C. Albertsson, *Biomacromolecules* 11 (2010) 1067–1073.
- [16] S. Regnell Andersson, M. Hakkarainen, S. Inkinen, A. Södergård, A.-C. Albertsson, *Biomacromolecules* 13 (2012) 1212–1222.
- [17] H. Yamane, K. Sasai, *Polymer* 44 (2003) 2569–2575.
- [18] G. Vitulli, C. Evangelisti, A.M. Caporusso, P. Pertici, N. Panziera, S. Bertozzi, P. Salvadori, in: B. Corain, G. Schmid, N. Toshima (Eds.), *Metal Nanoclusters in Catalysis and Materials Science: The Issue of Size Control*, Elsevier, Amsterdam, 2008 (Chapter 32).

- [19] C. Evangelisti, N. Panziera, A. D'Alessio, L. Bertinetti, M. Botavina, G. Vitulli, *J. Catal.* 272 (2010) 246–252.
- [20] K.J. Klabunde, *Free Atoms, Clusters and Nanoscale Particles*, Academic Press, San Diego, 1994.
- [21] D.A. Shirley, *Phys. Rev. B* 5 (1972) 4709–4714.
- [22] G. Giachi, M. Frediani, W. Oberhauser, E. Passaglia, *J. Polym. Sci. Part A: Polym. Chem.* 49 (2011) 4708–4713.
- [23] H.R. Kricheldorf, I. Kreiser-Saunders, C. Boettcher, *Polymer* 36 (1995) 1253–1259.
- [24] G. Giachi, W. Oberhauser, M. Frediani, E. Passaglia, L. Capozzoli, L. Rosi, *J. Polym. Sci. Part A: Polym. Sci.* 51 (2013) 2518–2526.
- [25] A. Södergård, M. Niemi, J.-F. Selin, J.H. Näsman, *Ind. Eng. Chem. Res.* 34 (1995) 1203–1207.
- [26] J.L. Espartero, I. Rashkov, S.M. Li, N. Manolova, M. Vert, *Macromolecules* 29 (1996) 3535–3539.
- [27] D. Brizzolara, H.-J. Cantow, K. Diederichs, E. Keller, A.J. Domb, *Macromolecules* 29 (1996) 191–197.
- [28] D. Sawai, Y. Tsugane, M. Tamada, T. Kanamoto, M. Sungil, S.-H. Hyon, *J. Polym. Sci. Part B: Polym. Phys.* 45 (2007) 2632–2639.
- [29] J. Lu, P.H. Toy, *Chem. Rev.* 109 (2009) 815–838.
- [30] Y. Uozumi, R. Nakao, *Angew. Chem. Int. Ed.* 42 (2003) 194–197.
- [31] E.H. Voigt, A.J.M. Mens, O.L.J. Gijzeman, J.W. Geus, *Surf. Sci.* 350 (1996) 21–31.
- [32] M. Brun, A. Berthet, J.C. Bertolini, *J. Electron Spectrosc. Relat. Phenom.* 104 (1999) 55–60.
- [33] J. Zhang, H. Sato, H. Tsuji, I. Noda, Y. Ozaki, *Macromolecules* 38 (2005) 1822–1828.
- [34] J.S. Struki, J.L. Walter, *Spectrochim. Acta* 27A (1971) 209–221.
- [35] G. Villain, A. Gaset, Ph. Kalck, *J. Mol. Catal. A: Chem.* 12 (1981) 103–111.
- [36] J.-Y. Lee, Y. Liao, R. Nagahata, S. Horiuchi, *Polymer* 47 (2006) 7970–7979.
- [37] A. Borodziński, M. Bonarowska, *Langmuir* 13 (1997) 5613–5620.
- [38] A. Giroir-Fendler, D. Richard, P. Gallezot, *Catal. Lett.* 5 (1990) 175–182.
- [39] C. Minot, P. Gallezot, *J. Catal.* 123 (1990) 341–348.
- [40] N. Yan, C. Xiao, Y. Kou, *Coord. Chem. Rev.* 254 (2010) 1179–1218.
- [41] N. Yan, Y. Yuan, P.J. Dyson, *Dalton Trans.* 42 (2013) 13294–13304.
- [42] A. Roucoux, J. Schulz, H. Patin, *Chem. Rev.* 102 (2002) 3757–3778.
- [43] J.I. Langford, A.J.C. Wilson, *J. Appl. Cryst.* 11 (1978) 102–113.
- [44] S. Miao, C. Zhang, Z. Liu, B. Han, Y. Xie, S. Ding, Z. Yang, *J. Phys. Chem. C* 112 (2008) 774–780.
- [45] B.M. Choudary, S. Madhi, N.S. Chowdari, M.L. Kantam, B. Sreedhar, *J. Am. Chem. Soc.* 124 (2002) 14127–14136.
- [46] K. Zhou, Y. Li, *Angew. Chem. Int. Ed.* 51 (2012) 602–613.
- [47] K. An, G.A. Somorjai, *ChemCatChem* 4 (2012) 1512–1524.